Journal of Digital Imaging

Analysis of the Glomerular Basement Membrane in Images of Renal Biopsies Using the Split-and-Merge Method: A Pilot Study

Ilya Kamenetsky,[1] Rangaraj M. Rangayyan,[1] and Hallgrimur Benediktsson[2]

Abnormal thinning, thickening, or variation in the thickness of the glomerular basement membrane (GBM) are caused by familial hematuria, diabetes mellitus, and Alport syndrome, respectively. We propose a semi-automated procedure for the segmentation and analysis of the thickness of the GBM in images of renal biopsy samples obtained by using a transmission electron microscope (TEM). The procedure includes the split-and-merge algorithm, morphological image processing, skeletonization, and statistical analysis of the width of the GBM. The procedure was tested with 34 TEM images of six patients. The mean and standard deviation of the GBM width for a patient with normal GBM were estimated to be 368±177 nm, those for a patient with thin GBM associated with familial hematuria were 216±95 nm, and those for a patient with thick GBM due to diabetic nephropathy were 1,094±361 nm. Comparative analysis of the results of image processing with manual measurements by an experienced renal pathologist indicated low error in the range of 12±9 nm.

KEY WORDS: Glomerular basement membrane, split-and-merge algorithm, skeletonization, segmentation, morphological image processing

INTRODUCTION

The Glomerular Basement Membrane

The kidney is a part of the urinary system responsible for the excretion of the body's waste products and for maintaining the proper balance of water and electrolytes in the blood. The functional unit of the kidney, the nephron, comprises the renal corpuscle and the renal tubule. The renal corpuscle, in turn, includes Bowman's capsule and the glomerulus, where the filtering of selected blood components occurs.[1,2] The filtering action within the glomerulus is performed by endothelial cells, the glomerular basement membrane (GBM), and the visceral epithelium (podocytes), which together prevent the passage of negatively charged molecules larger than albumin (about 3.6 nm) through the barrier.[3]

The GBM plays a crucial role in both structural support and functional operation of the glomerulus. The GBM is built of a meshwork of fused basal lamina mainly composed of laminin and collagen IV, and is divided into three layers: the lamina rara interna, the lamina densa, and the lamina rara externa. The typical width of the GBM is twice the thickness of most of human basement membranes, and is usually in the range of 300–350 nm.[1,2]

Imaging and Analysis of the GBM for the Diagnosis of Renal Pathology

Analysis of transmission electron microscopy (TEM) images of renal biopsy samples is an important tool for the diagnosis of diseases such as essential hematuria and thin-basement-membrane nephropathy,[4–6] Alport syndrome (AS),[7,8] and diabetes mellitus.[9,10]

Hematuria is defined as the presence of red blood cells in the urine, which can result from

[1]*From the Department of Electrical & Computer Engineering, Schulich School of Engineering, University of Calgary, Calgary, AB, T2N 1N4, Canada.*

[2]*From the Department of Pathology & Laboratory Medicine, University of Calgary, Calgary, AB, T2N 1N4, Canada.*

Correspondence to: Rangaraj M. Rangayyan, Department of Electrical & Computer Engineering, Schulich School of Engineering, University of Calgary, Calgary, AB, T2N 1N4, Canada; tel: +1-403-220-6745; e-mail: ranga@ucalgary.ca

Online publication 4 September 2009

doi: 10.1007/s10278-009-9233-5

bleeding at any level of the urinary tract. Glomerular hematuria usually indicates glomerular disease, such as inflammation (glomerulonephritis), or basement membrane abnormality, such as thin membranes or AS. Pathological changes of the GBM in patients with hematuria include thinning to the range of 100–200 nm with occasional disruption and breaks.[2]

For patients with AS, the typical lesion is characterized by irregular thickening of the GBM to the range of 800 to 1,200 nm, with splitting and fragmentation of the lamina densa, sometimes alternating with thinning of some portions of the GBM to the range of 100–200 nm. In early or mild cases of AS, thinning may be the predominant feature.

Diabetic nephropathy is a microvascular disease of the glomerulus that affects patients with type 1 and 2 diabetes. Pathological changes in the glomerulus include diffuse thickening of the GBM accompanied by steady decline of the glomerular filtration rate. The pathogenesis of this alteration is poorly understood; it correlates with proteinuria and may be related to abnormal podocyte function.[3,11]

Although quantitative analysis of the GBM is of high importance to a pathologist, only a limited number of reliable techniques have been developed. The available techniques include the manual methods developed by Osawa et al.[12] and methods relying on a sampling grid superimposed on the micrograph.[5,6] Whereas these techniques can be applied to a limited dataset of images, the general use of the existing methods is subjective, time consuming, and prone to errors. Only a few image-processing methods[13,14,15] have been proposed to detect and analyze the GBM. The method proposed by Ong et al.[13] includes measures of smoothness, uniformity, intensity difference, and intensity continuity to track the center line of the GBM starting from a manually initialized point and direction, followed by region growing. Although Ong et al. provided the details of evaluation of the results by a pathologist, no results of clinical application were provided. Recently, we proposed methods based on morphological image processing and active contour models (ACM) for semiautomatic segmentation and analysis of the GBM.[15] The procedure was tested with 34 TEM images of six patients. Comparative analysis of the results with manual measurements by an experienced renal pathologist indicated low error in the range of 36±11 nm. However, weaknesses of the ACM-based method include the requirement of manual construction of walls to prevent leakage of the ACM contours, manual initialization of contours, and the complexity of the parameters affecting the deformation of the ACM contours.

In the present paper, we propose methods for semiautomatic and user-guided methods for objective, reliable, and quantitative analysis of the GBM thickness in TEM images of renal biopsy samples. The methods include steps for the split-and-merge (SAM) algorithm,[16] morphological image processing,[17] skeletonization,[16,18,19] and statistical analysis of the width of the GBM.[15,20]

METHODS

Image Acquisition

TEM[21] is extensively used in medical applications to reveal the ultrastructure of biological samples to the order of a few nanometers.[19,22] The images used in the present study were acquired by using a Hitachi H-7000 TEM system with magnification in the range of 1,500 to 17,000, and were digitally captured by an H-7000 4.2 MP (mega pixel) charge-coupled device camera with 8 bits per pixel. The computer used to process the images is a Dell Precision 360 workstation with the following characteristics: 3.20 GHz Pentium 4 processor, 2 MB of cache memory, and 2 GB of RAM. Figure 1a shows an example of a TEM image including parts of a GBM.

The dataset used in the present study includes 34 TEM images of renal biopsy samples of six patients: one patient with abnormally thin GBM, one with abnormally variable GBM width, two with normal GBM, and two with abnormally thick GBM. Some of the details of the six patients are listed in Table 1. For each patient, one image was selected for manual segmentation and analysis, with several regions of interest (ROIs) including sections of the GBM. The images were processed independently by an experienced renal pathologist (H.B.) and the proposed methods, including segmentation of the GBM, measurement of its width, and computation of the statistics for comparative analysis. The same dataset of images and

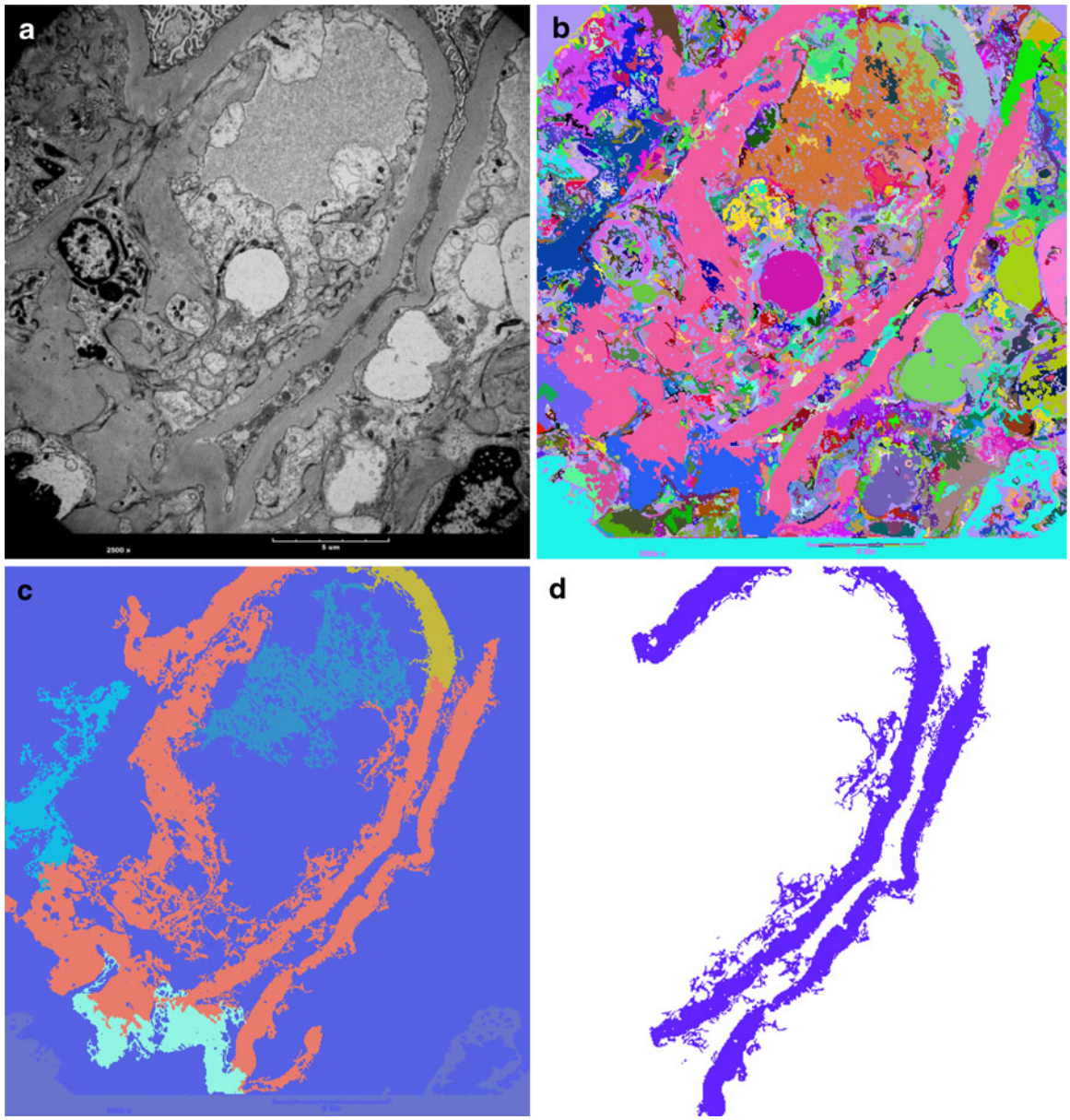

Fig. 1. a A TEM image of a renal biopsy sample. The true length of the *calibration bar* in the image is 5 μm. The size of the image is 485×512 pixels, with a resolution of 21.4 pixels/μm. b The result of application of the SAM algorithm to the image in (a). c Result of filtering by size and by shape applied to the image in (b). The large regions in the *lower left-hand corner* of the image represent parts of collapsed GBM. d The result in (c) after marking the regions corresponding to the GBM and removal of artifacts.

manual measurements as reported in our previous related report[15] were used in the present study.

Segmentation of the GBM Using the Split-and-Merge Method

The method proposed in the present work for segmentation and analysis of the GBM includes the following steps in the SAM algorithm[16] and additional morphological image-processing techniques for post-processing:[17]

1. Set the entire image as an initial region.
2. Split the region into a number of subregions (equal to four in the present work).
3. For each subregion, check if it satisfies a homogeneity criterion. For those that do not, go to Step (2).

Table 1. Description of the Patients and TEM Images used in the Present Work

Patient	Gender, age	Number of images	GBM distribution	Diagnosis
1	f, 60	6	Abnormally thin	Hematuria
2	f, 63	6	Abnormally variable	Hematuria and diabetes mellitus
3	f, 31	5	Normal	IgA nephropathy
4	f, 86	6	Normal	IgA nephropathy
5	m, 39	5	Abnormally thick	Diabetic nephropathy
6	m, 43	6	Abnormally thick	Diabetic nephropathy

f female, *m* male, *IgA* immunoglobulin A. Age is given in years

4. Stop splitting when all regions satisfy the homogeneity criterion.
5. For each subregion, check the neighboring regions. If they can be merged such that the united region will satisfy the homogeneity criterion, perform merging.
6. Repeat Step (5) until all possible merges are done.
7. Reject regions based on size and shape.
8. If required, manually combine GBM segments and remove artifacts.
9. Apply morphological smoothing and opening by reconstruction.[16]

In the splitting procedure, to check whether a certain region is homogeneous, first, the gray-level variance of the pixels within the region is calculated; then, the result is compared with the value of the homogeneity threshold specified (set to 7 in the gray-scale range of [0, 255] in the present work). In the merging procedure, for each pixel within a region, the 8-connected neighborhood is checked to verify if there are other neighboring regions such that the absolute difference between the regions' means is less than a second homogeneity threshold (set to 11 in the present work).

A graphical user interface (GUI) has been developed in the present work to facilitate the execution of the methods described above, as well as the subsequent steps described in the following paragraphs. The GUI and all procedures were developed in MATLAB®.

Figure 1b shows the result of application of the SAM method to the image in Figure 1a. As can be seen, most of the GBM has been recognized by the SAM algorithm as a relatively homogeneous region. In places where gray-level changes exceed the homogeneity threshold, parts of the GBM have been identified as separate segments. Such regions, if required for subsequent analysis, can be included manually by the operator. Another segmentation challenge is associated with the so-called collapsed GBM,[2] which is a part of the GBM corresponding to areas with lost podocytes, and should be excluded from further analysis. Due to the fact that both the collapsed and the normal GBM are of the same nature, and as a result, possess similar texture and brightness in TEM images, their separation cannot be achieved automatically. As seen from the SAM result in Figure 1b, the segmentation procedure cannot distinguish between these two types of tissue, and manual intervention of the operator is required to eliminate regions corresponding to collapsed GBM.

Due to the high complexity of TEM images of renal biopsy samples, the SAM procedure can produce a large number of segments. To limit the number of regions for further analysis, and to facilitate the operator in the recognition of the GBM, two types of filters are proposed. The part of the GUI related to the filtering step is shown in Figure 2. The first filtering technique is based on the fact that the GBM is a nearly uniform region with no abrupt discontinuities, and as a result, after application of the SAM procedure, should comprise one or a few relatively large segments. Filtering of regions by size is achieved by using a normalized threshold value τ_n that can be set in the range of [0, 1] in steps of 0.01. The default value of τ_n is set to 0.1. Then, the minimum size of the segments to be retained is calculated as

$$T = \alpha \tau_n MN, \tag{1}$$

where M and N are numbers of rows and columns in the preprocessed image, respectively, and α is an empirical coefficient that is set to be equal to

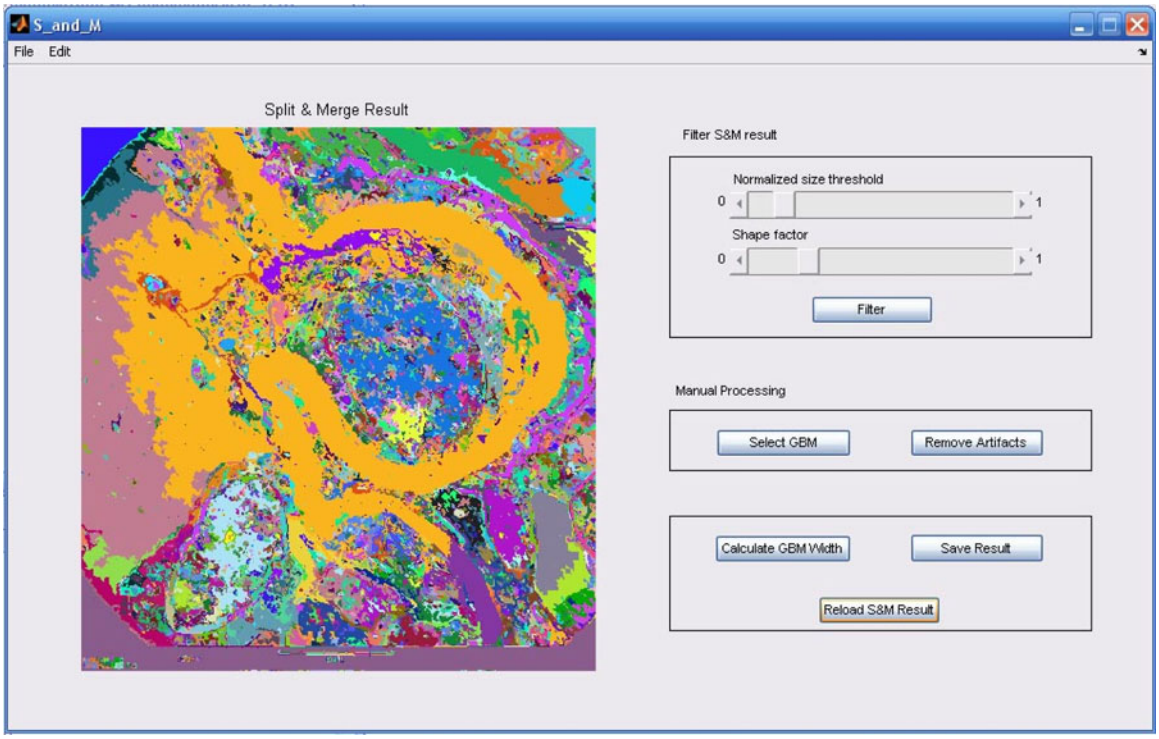

Fig. 2. GUI for filtering of regions based on size and shape in the proposed procedure for segmentation and analysis of the GBM. *S&M* **split-and-merge.**

0.05. If the procedure is to be applied to images with varying spatial resolution, an additional factor related to pixel size may be incorporated into the equation above.

The second filtering technique takes into account the shape of the GBM. The GBM is a narrow ribbon-like region, which, in comparison with other tissues present in TEM images, has higher compactness,[19] defined as

$$cf = -1\frac{4\pi A}{P^2}. \qquad (2)$$

Here, A is the area and P is the perimeter of the region being processed. The normalized definition of compactness results in a value of unity for a straight line (with the area contained being zero) and zero for a circle. The operator can set a threshold value of compactness in the range of [0, 1] in steps of 0.01: a threshold of 0 will preserve all shapes except circles, and a threshold of 1 will reject all regions. The default value for the compactness threshold is set to 0.2.

In most TEM images, the brightness of the GBM does not remain the same and can vary within the image. Therefore, after application of the SAM method, the GBM will comprise several regions of different size and shape. Manual selection of the filtering thresholds gives the user flexibility to achieve trade-off between the precision of the result and the operational time; see the GUI shown in Figure 2. If a rough estimate is adequate, the user can set high filtering thresholds, so that most of the non-GBM regions along with some of the GBM segments will be removed. To include most of the GBM regions in the analysis, the filtering thresholds should be set low; however, more subsequent manual processing may be required. Figure 1c shows the result of filtering with relatively high thresholds (equal to 0.5 for τ_n and 0.94 for cf). This way, minimal or no intervention is required from the operator to finalize the selection of the GBM to produce a result similar to that shown in Figure 1d.

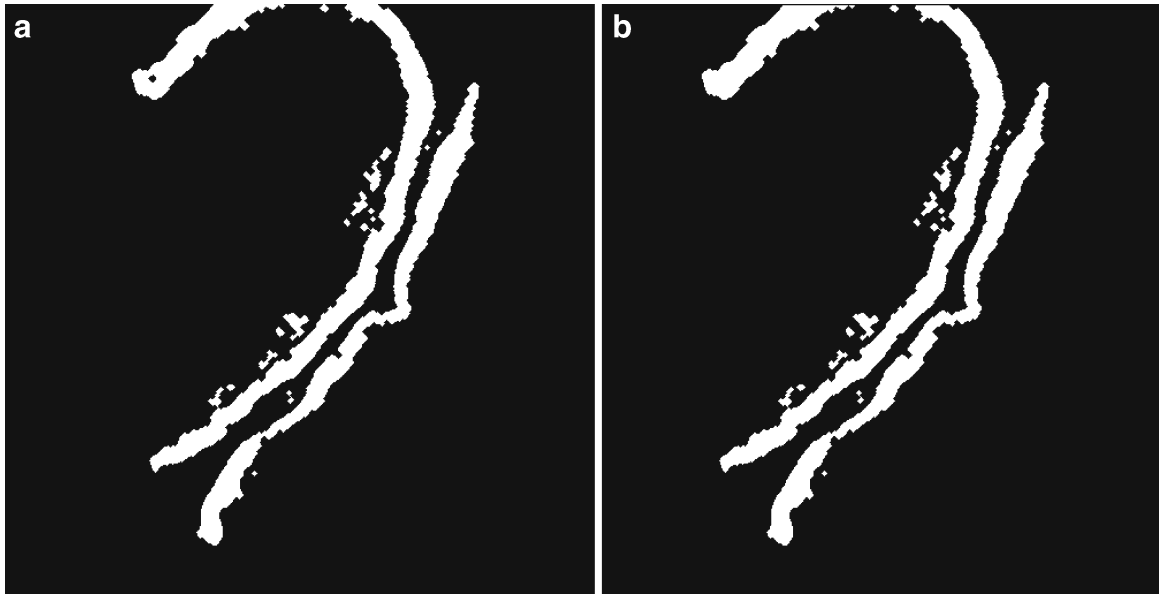

Fig. 3. a The result of morphological smoothing of the image in Figure 1d with a disc-shaped structuring element of radius 2 pixels. b The result of opening by reconstruction of the image in (a).

After application of the SAM algorithm and subsequent filtering of the result, the segmented region(s) should correspond to the GBM tissue present within the image, as shown in Figure 3a for the original image and the preprocessed versions in Figure 1. However, it was observed that the regions included holes and were surrounded by a connected mesh-type network of pixels that were falsely recognized to be part of the GBM. The causes of these artifacts are the intensity variations present within the GBM and also the absence of sharp boundaries of the GBM. To eliminate these artifacts, the morphological smoothing operation is applied, which consists of the morphological opening operator followed by the closing operator.[17] Figure 3a shows the result of morphological smoothing applied to the image in Figure 1d. However, this step does not fill holes of size larger than the structuring element (defined as a disk of radius 2 pixels in the present work). To overcome this limitation, opening by reconstruction[17] is applied to the result of morphological smoothing. The marker for the reconstruction step is chosen to be a black square of the size of the image, placed within a white frame of unit-pixel width. The mask is set to be equal to a binary negative of the image surrounded in a similar manner by a white frame. Figure 3b gives an example of the result of application of opening by reconstruction to the result of morphological smoothing shown in Figure 3a.

Skeletonization of the GBM

After most of the GBM tissue present in the image being analyzed has been segmented, the results of segmentation are passed on to a procedure for the detection of the skeleton.[15,16,18,19] The skeleton is a binary, 1-pixel-wide representation of the given image that summarizes information related to the size, orientation, shape, and connectivity of the objects in the image. A point $h \in F$ belongs to the skeleton of F, if, for the largest disc centered at h, expressed as $D(h)$, there does not exist a disc D, such that $D(h) \subset D \subseteq F$.[16,18] The skeleton of the segmented GBM shown in Figure 3b is displayed in Figure 4a.

In addition to pixels corresponding to the central line of the GBM, the skeletons obtained using the procedure described above were observed to contain several short segments due to the presence of protrusions, incursions, and minor details in the GBM (see Fig. 1a and Fig. 4a). Such spurs or hair-like parts of the skeleton, if left intact, could lead to erroneous measurements of the GBM width and

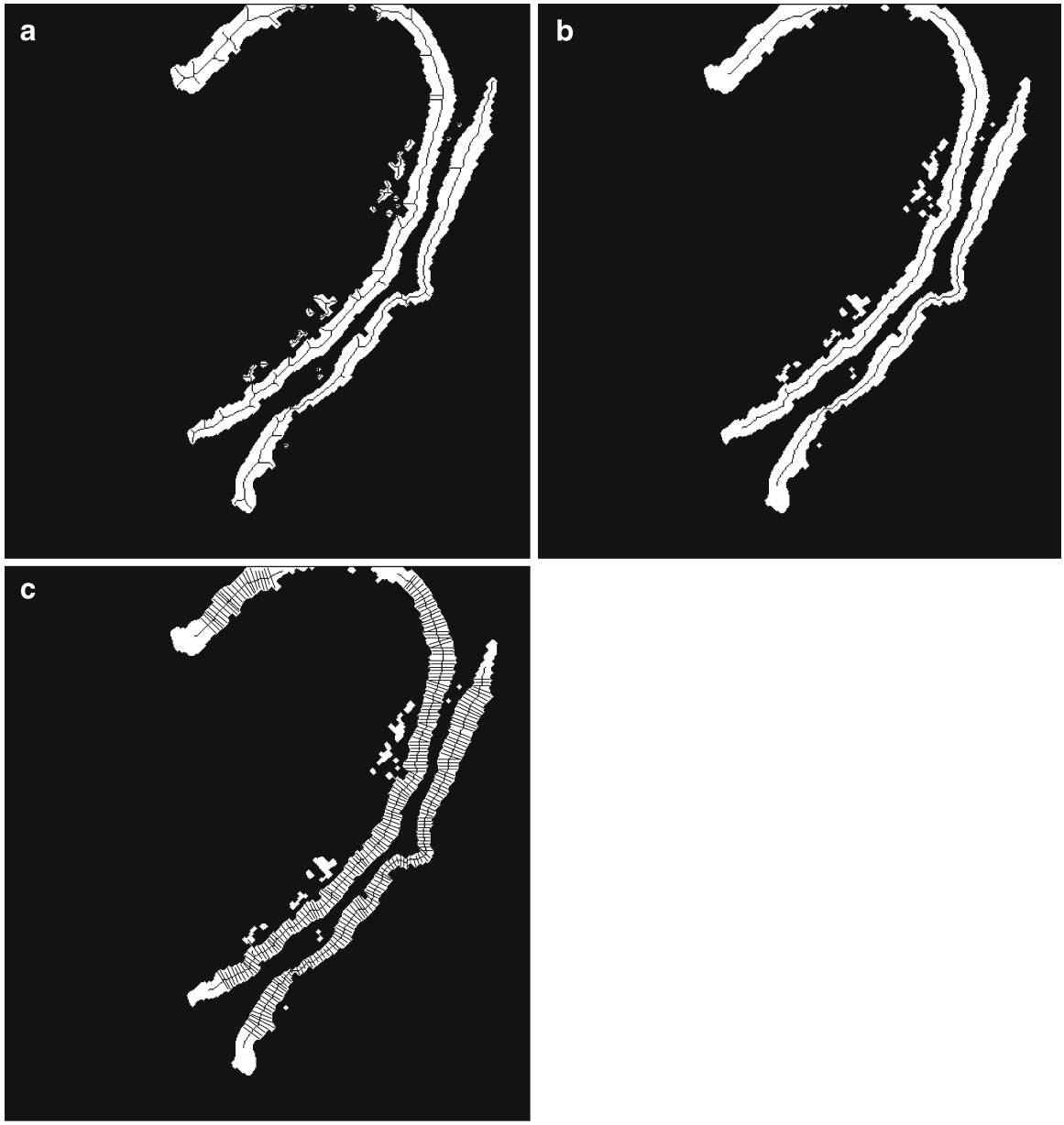

Fig. 4. a Skeletons derived from the segmented GBM region shown in Figure 3b. b The skeletons after trimming of spurs. c Measurement of the GBM width in directions perpendicular to the skeleton of each contour. For the sake of clarity, the measurement lines are shown only for every third pixel.

therefore should be removed. The technique of "skeleton shaving"[17] was applied for this purpose. When applied once, the procedure removes a single pixel at each end of the skeleton. If the procedure is repeated N_s times, where N_s is called the "shaving depth", such that N_s is larger than the length of the spurs, the remaining skeleton corresponds to the central line of the GBM. Figure 4b shows the result of "skeleton shaving" of the skeletons in Figure 4a, with a "shaving depth" N_s= 23 pixels. It is seen that most of the spurs have been trimmed or removed. This procedure results in the loss of a few points, as determined by the value of N_s used, at the ends of each GBM segment. In the

Table 2. Comparison of the Results Obtained with the Proposed SAM Method and Manual Measurements Performed by the Pathologist

	Manual		SAM	
Patient	μ	σ	μ	σ
1	164	60	189	39
2	393	106	374	123
3	205	42	208	37
4	442	118	426	156
5	1,173	213	1,175	255
6	1,109	237	1,115	302

μ and σ represent the mean and standard deviation of the GBM width in nanometers

present work, such a loss was considered to have negligible effect on the final results of statistical analysis.

The pixels of a given skeleton need to be linked together with the skeleton's chains. The linking procedure starts at one of the skeleton's ends, and is carried on using the 8-connected neighborhood until the other end is detected. If, during the linking procedure, the skeleton splits into two or more branches, the linking for the current chain is terminated, and the pixels corresponding to the beginnings of each branch are added to the list of the skeleton's end points to form their own skeleton chains. Because a GBM image can comprise several disconnected regions, there can be many skeleton chains formed at the end of the linking procedure. The process ends when all skeleton points get linked to the skeleton chains. Upon completion of the linking procedure, the length of each skeleton chain is checked against the minimum length threshold. If a chain's length is less than the specified minimum size (equal to 21 pixels in the present work), it is removed. The minimum-length limit was determined based upon the characteristics of the typical images in the dataset processed. The low limit set ensures that significant portions of the GBM are not deleted.

Measurement and Analysis of the Width of the GBM

The following procedure is applied for the estimation of the GBM width:[15]

1. Start with the first skeleton chain.
2. Denote by w the size of a sliding window and by l a chain's length. Place the sliding window at the beginning of the chain such that the first w elements of the chain are included in the analysis.
3. Fit a straight line to all the pixels within the sliding window and calculate its slope t.
4. Estimate the slope of the normal to the composed line as $n=-1/t$. If t is less than a

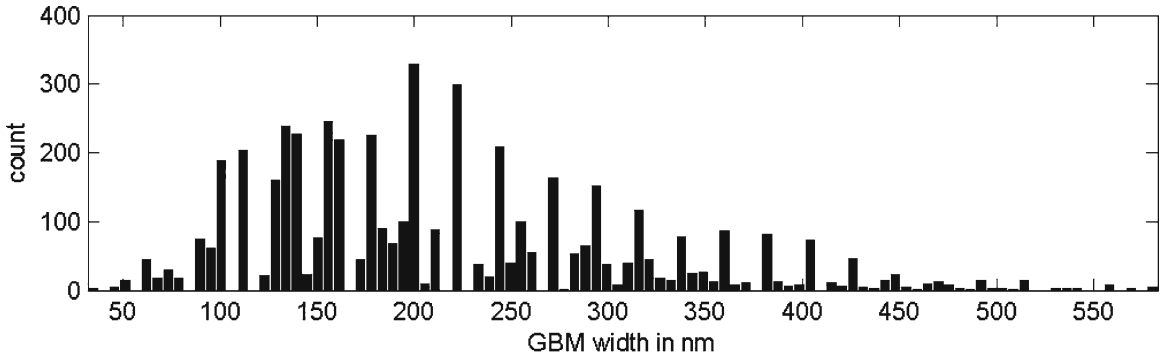

Fig. 5. Cumulative histogram of the GBM width for the first patient, with abnormally thin GBM due to hematuria, using the SAM method with 16 ROIs from six TEM images.

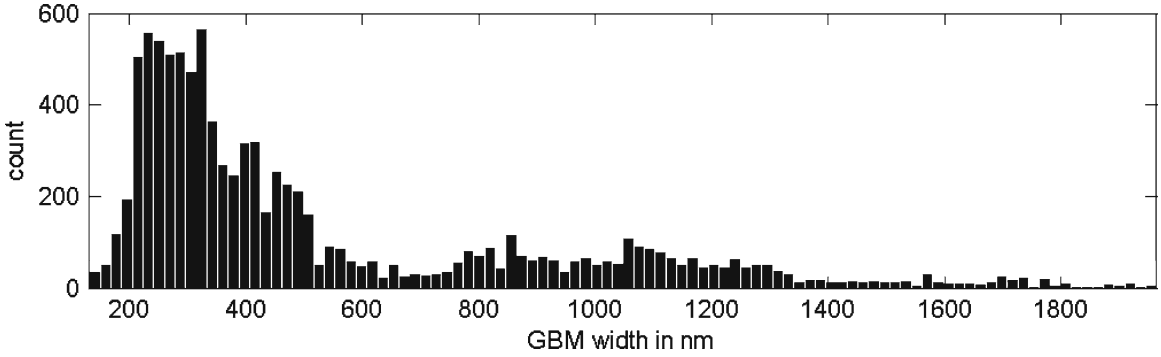

Fig. 6. Cumulative histogram of the GBM width for the second patient, with abnormally variable GBM due to hematuria and diabetes mellitus, using the SAM method with 14 ROIs from six TEM images.

minimum slope threshold (equal to 0.2 in the present work), mark n as a vertical line.

5. Using the slope of the normal n and the pixel corresponding to the center of the sliding window, build the equation to the line perpendicular to the straight-line fit obtained in Step (3).
6. Follow the perpendicular line in both directions from the skeleton pixel until the boundary of the GBM region is reached. If, during the growth procedure, the perpendicular line touches the image boundary or intersects with another skeleton point, discard the line.
7. Calculate the Euclidean distance between the two end points, corresponding to the intersections of the perpendicular line with the GBM boundary.
8. If the position of the sliding window is less than $l-w/2$, advance it by 1 to the next skeleton point and go to Step (3); otherwise proceed to the next skeleton chain and go to Step (2).

Figure 4c depicts the width measurements along the GBM using the skeleton shown in Figure 4b. The histogram of all of the GBM width measurements is accumulated for the case being processed, which could include several ROIs from several images. The following steps are then applied for analysis of the GBM:[15]

1. conversion of the width data from pixels to nm;
2. calculation of the mean (μ) and the standard deviation (σ);
3. rejection of the width values outside the range $[\mu \pm 2\sigma]$;
4. recalculation of μ and σ;
5. estimation of skewness, kurtosis, and coefficient of variation (CV$=\sigma/\mu$);
6. plotting of the histogram of the GBM width measurements; and
7. updating the accumulated statistics.

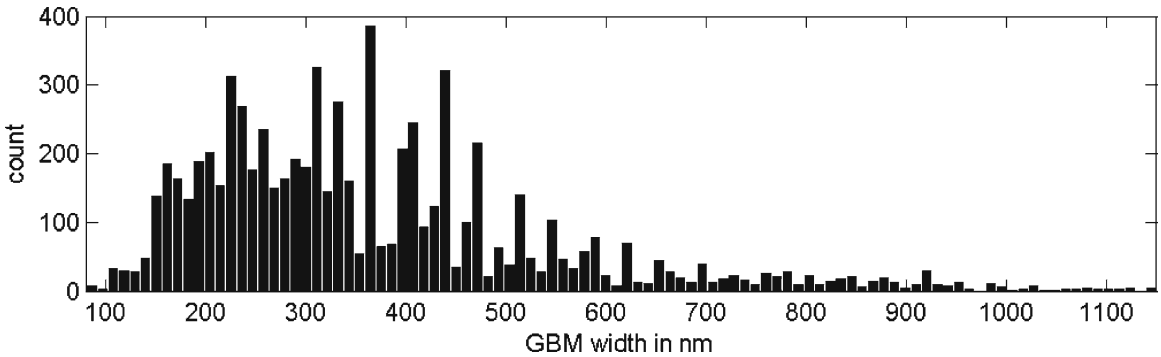

Fig. 7. Cumulative histogram of the GBM width for the third patient, with normal GBM, using the SAM method with 11 ROIs from five TEM images.

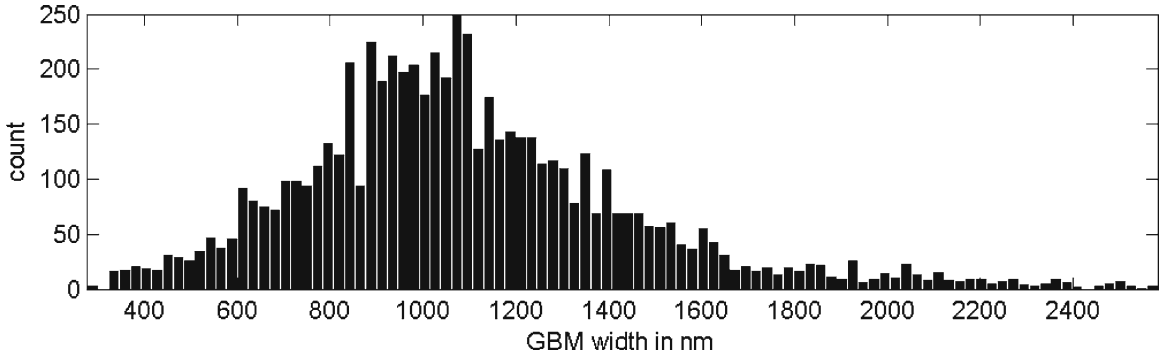

Fig. 8. Cumulative histogram of the GBM width for the fifth patient, with abnormally thick GBM due to diabetic nephropathy, using the SAM method with 11 ROIs from five TEM images.

The GUI developed for the present work facilitates the application of the methods described above.

EXPERIMENTS AND RESULTS

The proposed methods were tested with 34 TEM images of six patients; see Table 1 and 'Image Acquisition' section for details. All image-processing experiments were conducted by the same individual (I.K.). Compared with manual measurements performed by an experienced renal pathologist (H.B.) on one image each of the six patients studied, the average and standard deviation of the differences in the mean widths provided by the SAM method were 12±9 nm; see Table 2 for details. The performance of the SAM method is superior to that of another method that we recently proposed for the same application, based on morphological image processing and active contours,[15] which had an error of 36±11 nm with respect to manual measurements using the same set of images.

The accumulated histograms for four of the six patients in the study are shown in Figures 5, 6, 7, and 8. The statistics computed for all of the six patients in the study are shown in Table 3. The mean and standard deviation of the GBM width for one of the patients with normal GBM were estimated to be 368± 177 nm, those of a patient with thin GBMs associated with familial hematuria were 216±95 nm, and those of a patient with thick GBM due to diabetes were 1,094±361 nm. For one of the patients with hematuria and diabetic nephropathy, demonstrating abnormally variable GBM width, the mean and standard deviation of the GBM width were 533±371 nm, leading to the highest coefficient of variation observed (in the present study) of CV=0.7.

DISCUSSION AND CONCLUSION

A semi-automatic procedure for the segmentation and analysis of the GBM has been presented

Table 3. Cumulative Statistics of the GBM Width Distribution Obtained with the Proposed SAM Method

			Statistics of GBM Width				
Patient	Number of images	Number of ROIs	μ	σ	S	K	CV
1	6	16	216	95	0.9	3.5	0.4
2	6	14	533	371	1.4	4.2	0.7
3	5	11	368	177	1.3	5.1	0.5
4	6	17	407	173	1.0	3.9	0.4
5	5	11	1,094	361	0.9	4.5	0.3
6	6	17	1,056	433	1.1	4.8	0.4

The symbols μ, σ, S, K, and CV represent, respectively, the mean, standard deviation, skewness, kurtosis, and coefficient of variation. μ and σ are in nanometers

in this paper. The present study represents a pilot study with a small dataset of images to illustrate the nature of the problem and a potential solution. A limitation of the proposed procedure lies in the use of a few parameters that were set based upon experimentation with a few images; methods need to be developed to derive the required parameters automatically and to make the procedure fully automatic. Although fully automated methods for the detection and analysis of the GBM would be desirable in the future, the techniques proposed in the present work require some intervention from the user to ensure accurate analysis of the GBM. This requirement increases the average time needed to process an image of the GBM, and demands some knowledge and experience from the operator. A single operator (I.K.) performed the analysis reported in the present work. Variability of the results due to variation between operators needs to be established in further studies.

An additional limitation is associated with the complexity of the implemented algorithms, which puts constraints on the computer hardware used. The average time required for the processing of an ROI of size of 512×512 pixels on the computer specified in 'Image Acquisition' section is 90 s. The average time taken by the pathologist (H.B.) for the analysis of a comparable image is 2–4 min; however, manual measurements of GBM width were performed at significantly fewer locations as compared to the automatic measurements.

The results of statistical analysis of GBM width for the six patients in the study agree with the clinically observed and expected distributions of the GBM width for each case, including abnormally thin, normal, abnormally variable, and abnormally thick GBM width. The present study demonstrates the viability of a semi-automated procedure for the segmentation and analysis of the GBM using the SAM method.

Further detailed analysis of the statistical distribution and parameters of the GBM, such as skewness and kurtosis, requires results from a larger database of images and cases. The present work represents a pilot study with a small set of cases and images. Further work is planned with a larger database of clinically proven cases. The proposed methods should reduce the effort required to analyze TEM images of renal biopsy samples, and lead to improved quantitative analysis of the GBM.

REFERENCES

1. Vize PD, Woolf AS, Bard JBL: The kidney, from normal development to congenital disease, London: Academic, 2003
2. Schwartz MM, Jennette JH, Olson JL, Silva FG: Pathology of the kidney, 6th edition. New York: Lippincott Williams & Wilkins, 2007
3. Moriya T, Groppoli TJ, Kim Y, Mauer M: Quantitative immunoelectron microscopy of type VI collagen in glomeruli in type I diabetic patients. Kidney International 59:317–323, 2001
4. Coleman M, David W, Haynes G: Glomerular basement membrane abnormalities associated with apparently idiopathic hematuria. Human Pathology 17:1022–1030, 1986
5. Saxela S, Davies DJ, Kirsner RLG: Thin basement membranes in minimally abnormal glomeruli. Clinical Pathology 43:32–38, 1990
6. Basta-Jovanovic G, Venkataseshan VS, Gil J: Morphometric analysis of glomerular basement membranes in thin basement disease. Clinical Nephrology 33:110–114, 1990
7. Gubler MC, Levy M, Broyer M: Alport's syndrome: a report of 58 cases and a review of the literature. The American Journal of the Medical Sciences 70:493–505, 1981
8. Habib R, Gubler MC, Hinglais N: Alport's syndrome: experience at Hospital Necker. Kidney International 11:20–28, 1982
9. Osterby R: Thin glomerular basement membrane nephropathy: incidence in 3471 consecutive renal biopsies examined by electron microscopy. Archives of Pathology and Laboratory Medicine 130:699–706, 2006
10. Osterby R: Morphometric studies of the peripheral glomerular basement membrane in early juvenile diabetes. I. Development of initial basement membrane thickening. Diabetologica 8:84–92, 1972
11. Li JJ, Kwak SJ, Jung DS, Kim JJ, Yoo TH, Ryu DR, Han SH, Choi HY, Lee JE, Moon SJ, Kim DK, Han DS, Kang SW: Podocyte biology in diabetic nephropathy. Kidney International Supplement S:36–42, 2007
12. Osawa G, Kimmelstiel P, Sailing V: Thickness of glomerular basement membranes. Clinical Pathology 45:7–20, 1966
13. Ong SH, Giam ST, Jayasooriah , Sinniah R: Adaptive window-based tracking for the detection of membrane structures in kidney electron micrographs. Machine Vision and Applications 6:215–223, 1993
14. Ong SH, Jin XC, Jayasooriah , Sinniah R: Image analysis of tissue sections. Computers in Biology and Medicine 26:269–279, 1996
15. Rangayyan RM, Kamenetsky I, Benediktsson H: Segmentation and analysis of the glomerular basement membrane in renal biopsy images using active contours: a pilot study. Journal of Digital Imaging, available online, doi:10.1007/s10278-009-9188-6, in press, 2009
16. Gonzalez RC, Woods RE: Digital image processing, 2nd edition. Upper Saddle River: Prentice Hall, 2002
17. Goutsias J, Batman S: Morphological methods for biomedical image analysis. pp. 175–272. In: Sonka M, Fitzpatrick JM Eds. Handbook of medical imaging, volume 2: medical image processing and analysis. Bellingham: SPIE, 2000
18. Blum H: A transformation for extracting new descriptors of shape. In: Wathen-Dunn W (Ed.) Models for the perception of speech and visual form. Cambridge: MIT Press, 1967

19. Rangayyan RM: Biomedical image analysis, Boca Raton: CRC, 2005

20. Kamenetsky I, Rangayyan RM, Benediktsson H: Segmentation and analysis of the glomerular basement membrane using the split and merge method. In 30th Annual International Conference of the IEEE Engineering in Medicine and Biology Society (EMBC 2008). Canada: Vancouver, British Columbia, 2008, pp. 3064–3067

21. Bozzola JJ, Russell LD: Electron microscopy: principles and techniques for biologists, 2nd edition. Sudbury: Jones and Bartlett, 1999

22. Wgrowska-Danilewicz M, Danilewicz M: Current position of electron microscopy in the diagnosis of glomerular diseases. Polish Journal of Pathology, 58:87–92, 2007